

Citation for published version:
Genc, G & Rees, DAS 2011, 'The onset of convection in horizontally partitioned porous layers', *Physics of Fluids*, vol. 23, no. 6, 064107. https://doi.org/10.1063/1.3589864

DOI:
10.1063/1.3589864

Publication date:
2011

Link to publication

This article appeared in Genc, G. and Rees, D. A. S., 2011. The onset of convection in horizontally partitioned porous layers. Physics of Fluids, 23 (6), 064107 and may be found at http://dx.doi.org/10.1063/1.3589864

University of Bath

General rights
Copyright and moral rights for the publications made accessible in the public portal are retained by the authors and/or other copyright owners and it is a condition of accessing publications that users recognise and abide by the legal requirements associated with these rights.

Take down policy
If you believe that this document breaches copyright please contact us providing details, and we will remove access to the work immediately and investigate your claim.

Download date: 26. Feb. 2020

The onset of convection in horizontally partitioned porous layers

Gamze Genç[1,2] and D. Andrew S. Rees[2]
[1]*Mechanical Engineering, University of Erciyes, 38039 Kayseri, Turkey*
[2]*Mechanical Engineering, University of Bath, Bath, BA2 7AY, United Kingdom*

(Received 26 July 2010; accepted 12 April 2011; published online 22 June 2011)

In this paper, the onset of convection in a horizontally partitioned porous layer is investigated. Two identical sublayers are separated by a thin impermeable barrier. There exists a background horizontal flow in one of the layers or, equivalently, flows of half that strength in each sublayer but in opposite directions. A linearised stability analysis is performed where the horizontal component of the disturbance is factored into separate Fourier modes, leaving an ordinary differential eigenvalue problem for the critical Darcy-Rayleigh number as a function of the wavenumber. The dispersion relation is derived and the neutral stability curves are obtained for a wide range of horizontal flow rates. The presence of the horizontal flow alters the morphology of the neutral curves from that which occurs when there is no flow and travelling modes may arise. We also determine the condition under which the most dangerous disturbance changes from a stationary mode to travelling mode. Some three-dimensional aspects are also considered. © *2011 American Institute of Physics*. [doi:10.1063/1.3589864]

I. INTRODUCTION

Convection in a horizontal porous layer heated from below is now regarded as one of the classical and fundamental problems in stability analysis even though it also has a considerable importance in engineering applications such as CO_2 sequestration, oil recovery techniques, insulation technology, packed-bed catalytic reactors, and heat storage beds. Termed the Horton-Rogers-Lapwood or Darcy–Bénard problem, Horton and Rogers[1] and Lapwood[2] were the first to show that convection arises in a uniform unbounded horizontal layer heated from below occurs when the Darcy-Rayleigh number is above $4\pi^2$. The corresponding wavenumber is π, which means that the cells which first appear have a unit aspect ratio.

Prats[3] investigated the effect of a uniform horizontal pressure gradient on the onset problem for the Darcy-Bénard problem and found that the resulting horizontal flow does not affect the critical Rayleigh number. The full governing equations, when written in a frame of reference which moves with the flow, remain identical to those which apply when the flow is absent. Therefore, all the nonlinear dynamics which arise for the classical Darcy-Bénard problem in an unbounded layer are unchanged by the presence of the flow. No doubt that the presence of Brinkman effects and Local Thermal Nonequilibrium will alter this conclusion, but analysis of these types have not yet appeared in the open literature.

Layered porous media are ubiquitous both in nature and industrial applications, and numerous studies have been made of these cases. Although it was not the first paper on the topic, a very comprehensive analysis of the onset of convection was undertaken by McKibbin and O'Sullivan,[4] who considered two- and three-sublayer configurations. It was found that the neutral curve sometimes exhibits two local minima thereby allowing the identity of the critical mode of convection to change discontinuously as the system parameters change smoothly. This work was later extended into the weakly nonlinear regime by McKibbin and O'Sullivan.[5] Rees and Riley[6] also provided a weakly nonlinear stability analysis and showed that some configurations give rise naturally to three-dimensional convection patterns. A similar conclusion was obtained earlier by Riahi,[7] who considered a classical Darcy-Bénard layer sandwiched between two conducting solid regions. Other notable works on layered media have been undertaken by Masuoka *et al.*[8] and Rana *et al.*[9]

McKibbin[10] investigated the effects of the presence of an impermeable but conducting layer interposed between the heat source below and the base of an otherwise homogeneous aquifer. He found that the presence of a layer of impermeable material between the heat source and the saturated layer markedly affects the aspect ratio of convection cells and the heat flux when compared with those which occur when the heat source is in direct contact with the base of the aquifer. Another analysis of the linear stability characteristics of two horizontal porous layers separated by a conductive partition was undertaken by Jang and Tsai.[11] They showed that the system is at its most stable when the partition is located centrally, and the system also becomes more stable as the partition thickness increases or the partition conductivity decreases.

The aim of the present work is to determine the effect of the presence of a partition within a porous layer heated from below, and to allow different horizontal flows to exist within the two sublayers, which are caused by two different pressure gradients. The partition will be considered to be infinitesimally thin and completely impermeable so that the sublayers remain thermally coupled, but are mechanically decoupled. In addition, the sublayers are of identical thicknesses and properties. Given that the convection cells have a tendency to move with the background flow, the presence of different flows in each sublayer combined with the thermal coupling between the layers means that there will be a competition between the sublayers.

 © 2011 American Institute of Physics

Downloaded 01 Aug 2011 to 138.38.54.38. Redistribution subject to AIP license or copyright; see http://pof.aip.org/about/rights_and_permissions

The analysis we present is confined to a linearised stability theory, and we will show that the onset of convection may correspond either to a stationary pattern (when viewed in the correct frame of reference) or, when flow rates are sufficiently high, to two different travelling wave patterns. When one is not confined to two-dimensional flow and the background pressure gradients are not in the same direction, then it is possible to show that there is a roll direction which minimises the critical Darcy-Rayleigh number, and a simple formula is obtained for the direction of the axis of that roll.

II. GOVERNING EQUATIONS

The main aim of this study is to investigate the onset of convection within a uniform horizontal porous layer, which is heated isothermally from below and cooled isothermally from above, and within which a thin horizontal impermeable partition is placed; the configuration is as shown in Fig. 1.

When there is no applied horizontal pressure gradient, the basic state is one of no motion. We may, without any loss of generality, impose opposing pressure gradients in the two sublayers; any other situation may be reduced to this by the introduction of a suitable moving frame of reference in the manner of Prats.[3]

We assume that the Boussinesq approximation is valid and that the fluid motion satisfies Darcy's law with the additional effect of buoyancy. Initially, we consider only two-dimensional convection in the (x,z)-plane, as shown in Fig. 1, and the nondimensional governing equations are given by,

$$\frac{\partial u_j}{\partial x}+\frac{\partial w_j}{\partial z}=0, \tag{1}$$

$$u_j=-\frac{\partial p_j}{\partial x}, \qquad w_j=-\frac{\partial p_j}{\partial z}+Ra\,\theta_j, \tag{2}$$

$$\frac{\partial \theta_j}{\partial t}+u_j\frac{\partial \theta_j}{\partial x}+w\frac{\partial \theta_j}{\partial z}=\frac{\partial^2\theta_j}{\partial x^2}+\frac{\partial^2\theta_j}{\partial z^2}, \tag{3}$$

where u and w are the horizontal and vertical flux velocities, respectively, p is the pressure, θ the temperature, and t the time. The values $j=1,\ 2$ denote the identity of the sublayer, which is being considered. In the above, Ra is the Darcy-Rayleigh number:

$$\mathrm{Ra}=\frac{\rho(\rho C)_f\hat{g}\beta HK\Delta T}{\mu\kappa}. \tag{4}$$

Here, H is the height of a sublayer, rather than of the full layer (which has dimensional height, $2H$) and ΔT is the basic temperature drop across a sublayer. These choices have been made so that our results may be compared directly with the classical single-layer configuration. Moreover, ρ is the density, C the heat capacity, $\hat{g}$ gravity, β the coefficient of cubical expansion, K permeability, μ the dynamic viscosity, and κ the thermal diffusivity. Nondimensionalisation has taken place using H, $H^2(\rho C)_m/\kappa$, and $\kappa/H(\rho C)_f$ as scales of length, time, and velocity, respectively, where the subscripts f and m correspond to fluid and effective properties of the porous medium, respectively.

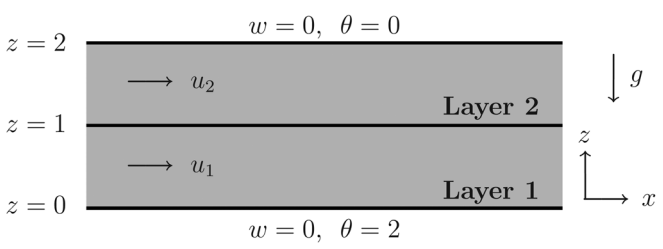


FIG. 1. Geometry of the horizontally partitioned porous medium.

The streamfunction ψ is defined using,

$$u_j=-\frac{\partial \psi_j}{\partial z}, \qquad w_j=\frac{\partial \psi_j}{\partial x}, \tag{5}$$

and, therefore, the non-dimensional equations take the following forms:

$$\begin{aligned}\frac{\partial^2\psi_j}{\partial x^2}+\frac{\partial^2\psi_j}{\partial z^2}&=\mathrm{Ra}\frac{\partial\theta_j}{\partial x},\\ \frac{\partial\theta_j}{\partial t}+\frac{\partial\psi_j}{\partial x}\frac{\partial\theta_j}{\partial z}-\frac{\partial\psi_j}{\partial z}\frac{\partial\theta_j}{\partial x}&=\frac{\partial^2\theta_j}{\partial x^2}+\frac{\partial^2\theta_j}{\partial z^2}.\end{aligned} \tag{6}$$

We impose different pressure gradients in the x-direction in the two sublayers and these are such that the basic velocity fields in the two sublayers,

$$u_1^{(b)}=\frac{1}{2}U, \qquad u_2^{(b)}=-\frac{1}{2}U, \tag{7}$$

where U is termed the velocity differential. Therefore, the equations are to be solved subject to the boundary and interface conditions,

$$\begin{aligned}&z=0: \quad \psi_1=0, \quad \theta=2,\\ &z=1: \quad \psi_1=\psi_2=\frac{1}{2}U, \quad \theta_1=\theta_2, \quad \frac{\partial\theta_1}{\partial z}=\frac{\partial\theta_2}{\partial z}.\\ &z=2: \quad \psi_2=0, \quad \theta=0.\end{aligned} \tag{8}$$

We note that the constant conditions for ψ_1 and ψ_2 express the fact that the interface and boundaries are impermeable, while the continuity conditions for the temperature and its vertical derivative at $z=1$ represent the fact that the conduction is unhindered by the presence of the partition.

III. LINEAR STABILITY ANALYSIS

The basic state consists of different uniform horizontal flows within the respective sublayers and a linear temperature drop, and it is

$$\theta_1^{(b)}=\theta_2^{(b)}=2-z, \quad \psi_1^{(b)}=\frac{1}{2}Uz, \quad \psi_2^{(b)}=\frac{1}{2}U(2-z). \tag{9}$$

The conditions governing the onset of convection are determined by using a linear stability analysis. Thus the basic solution is perturbed as follows; we substitute

$$\psi_j=\psi_j^{(b)}+\Psi_j, \qquad \theta_j=\theta_j^{(b)}+\Theta_j, \tag{10}$$

into Eq. (6), and then linearise for Ψ and Θ,

Downloaded 01 Aug 2011 to 138.38.54.38. Redistribution subject to AIP license or copyright; see http://pof.aip.org/about/rights_and_permissions

$$\frac{\partial^2 \Psi_j}{\partial x^2} + \frac{\partial^2 \Psi_j}{\partial z^2} = \mathrm{Ra}\frac{\partial \Theta_j}{\partial x},$$
$$\frac{\partial \Theta_j}{\partial t} + u_j^{(b)}\frac{\partial \Theta_j}{\partial x} - \frac{\partial \Psi_j}{\partial x} = \frac{\partial^2 \Theta_j}{\partial x^2} + \frac{\partial^2 \Theta_j}{\partial z^2}. \quad (11)$$

This partial differential system may be transformed into ordinary differential eigenvalue form by factoring out a horizontal Fourier mode with wavenumber, k, as follows:

$$\Psi_j = i f_j(z)\, e^{\lambda t + ikx} + \text{c.c.}, \quad \Theta_j = g_j(z)\, e^{\lambda t + ikx} + \text{c.c.}, \quad (12)$$

where c.c. denotes the complex conjugate and λ is the complex exponential growth rate. Equation (11) now becomes,

$$f_j'' - k^2 f_j = \mathrm{Ra}\, k\, g_j, \qquad g_j'' - k^2 g_j - iku_j^{(b)} g_j - kf_j = \lambda g_j, \quad (13)$$

subject to the boundary and interface conditions,

$$\begin{aligned} z = 0: &\quad f_1 = g_1 = 0, \\ z = 1: &\quad f_1 = f_2 = 0, \quad g_1 = g_2, \quad g_1' = g_2', \\ z = 2: &\quad f_2 = g_2 = 0. \end{aligned} \quad (14)$$

Equations (13) and (14) represent an eigenvalue problem for λ in terms of k and Ra. The solutions for f and g are complex when the velocity differential, U, is nonzero. When the real part of λ is zero then disturbances neither grow nor decay and this is termed neutral stability.

The neutral curves were obtained by a variety of methods, including (i) a suitably modified shooting method code coupled with a fourth order Runge-Kutta method, (ii) a matrix eigenvalue solver, which is applied after Eq. (13) was discretised by using a second order central difference formula on a uniform grid (see Rees and Bassom[12] for details), and (iii) the analytical determination of a complex dispersion relation (see Appendix A). In the case of the first method, it was necessary to adopt a normalization constraint of the form $g'(0) = 1$. The two numerical methods were used to verify the correctness of the somewhat complicated complex dispersion relation given in Eq. (A1) and therefore, we omit the details of their implementation. In the present paper, all our results were obtained by analysis of the dispersion relation and, therefore, our data are, to all intents and purposes, exact. Solutions were obtained using Newton-Raphson iteration with an extremely small convergence tolerance.

IV. TWO-DIMENSIONAL RESULTS FOR $U = 0$

When the velocity differential is zero, the dispersion relation may be found by attempting to solve Eq. (13) analytically. The application of the boundary and interface conditions, Eq. (14), results in the dispersion relation. We found that for even–numbered modes, we have

$$\sin\sigma_1 = 0, \quad (15)$$

while for odd numbered modes, we have

$$\sigma_1 \cos\sigma_1 \sinh\sigma_2 + \sigma_2 \cosh\sigma_2 \sin\sigma_1 = 0, \quad (16)$$

where the quantities, σ_1 and σ_2 are given by,

$$\sigma_1 = \sqrt{k\sqrt{Ra} - k^2}, \qquad \sigma_2 = \sqrt{k\sqrt{Ra} + k^2}. \quad (17)$$

Equation (15) yields the neutral curve for the classical single-layer Darcy-Bénard problem,

$$Ra = \frac{(k^2 + n^2\pi^2)^2}{k^2}, \quad \text{for } n = 1, 2, \ldots, \quad (18)$$

while Eq. (16) cannot be rearranged to yield Ra explicitly in terms of k.

Figure 2 shows the first four neutral modes. All the curves have a single minimum and Ra becomes asymptotically large as either $k \to 0$ or $k \to \infty$. Modes 2 and 4 correspond to the $n = 1$ and $n = 2$ Darcy-Bénard modes given by Eq. (18). Figure 3 shows the z-profiles for f and g for modes 1 and 2. The solutions are scaled in such a way that g has a unit slope on the lower surface. When the wavenumber is small, the thermal profile for mode 1 has a single maximum and has a shape which is similar to half of a sine wave. As k increases, the central part of the profile reduces until it has two identical maxima and a minimum at the interface. All the while, the streamfunction profile maintains the same sign and corresponds to a pair of stacked co-rotating cells. On the other hand, mode 2, being the usual mode 1 for the classical Darcy-Bénard problem, consists of a profile which is preciesly one period of a sine wave, and it corresponds to a stacked pair of counter-rotating cells.

The critical Darcy-Rayleigh number for mode 1 may be found easily by minimising the numerical value of Ra with respect to k; this process yields the value, $Ra_c = 2.74556\pi^2$, which should be compared with $4\pi^2$ for mode 2. The respective critical wavenumbers for modes 1 and 2 are $k/\pi = 0.74046$ and precisely 1. Thus, the convection pattern for mode 1 is approximately 35% wider than for mode 2.

Figure 2 also indicates that the neutral curves for modes 1 and 2 become very close indeed when k is large, which is

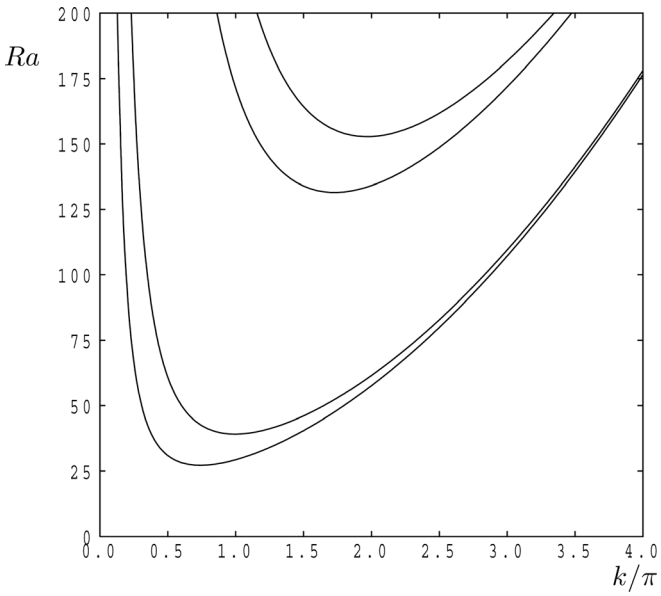


FIG. 2. The neutral curves corresponding to the first four modes of instability for $U = 0$.

Downloaded 01 Aug 2011 to 138.38.54.38. Redistribution subject to AIP license or copyright; see http://pof.aip.org/about/rights_and_permissions

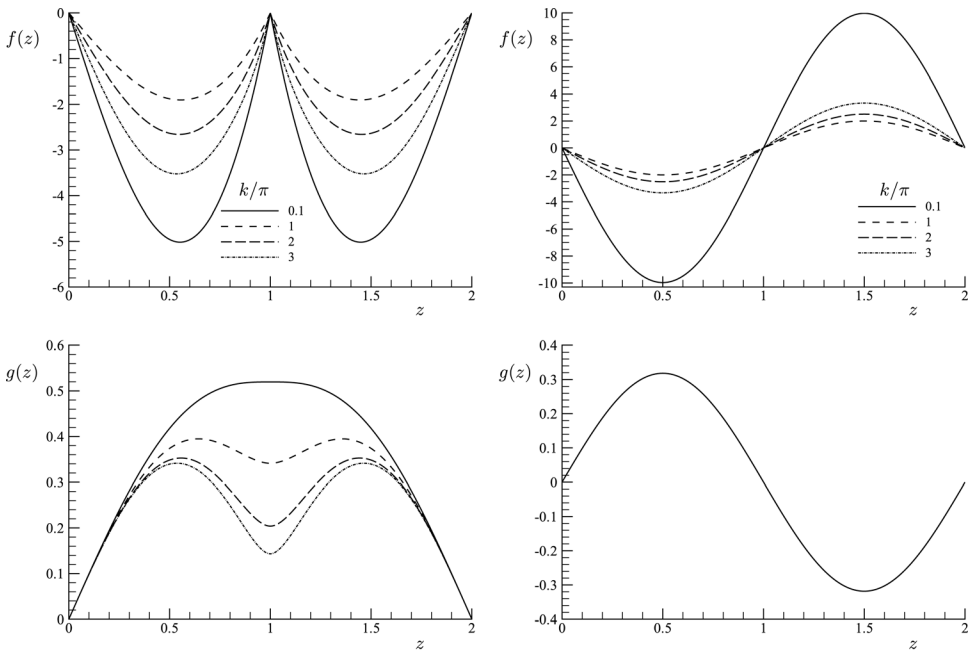


FIG. 3. Profiles of f and g for modes 1 and 2 for $U = 0$.

unusual behaviour. Using an asymptotic analysis of Eqs. (16) and (18), it is possible to show that the critical values of Ra_c have the forms,

$$\begin{aligned} Ra_c^{\text{Mode1}} &\sim k^2 + 2\pi^2 - 2\sqrt{2}\pi^2 k^{-1} + (\pi^4 + 3\pi^2)k^{-2}, \\ Ra_c^{\text{Mode2}} &= k^2 + 2\pi^2 \qquad\qquad + \pi^4 k^{-2}, \end{aligned} \tag{19}$$

when k is large, and therefore, the difference between these critical values is of $O(k^{-1})$. By contrast, the separation between different curves for the classical Darcy-Bénard layer is of $O(1)$ when k is large.

The observed behaviour of both f and g for mode 1, when k is large, suggests that a large- k analysis should be performed. We found that

$$\text{Mode1: } f_1 \sim -k\sin\pi z, \quad f_2 \sim k\sin\pi z, \quad g_1 \sim \sin\pi z, \quad g_2 \sim -\sin\pi z, \tag{20}$$

$$\text{Mode2: } f_1 \sim -k\sin\pi z, \quad f_2 \sim -k\sin\pi z, \quad g_1 \sim \sin\pi z, \quad g_2 \sim \sin\pi z, \tag{21}$$

when $k \gg 1$. These expressions have been normalised so that the mode 1 and mode 2 solutions are identical in the lower layer, i.e., layer 1, but the consequence is that they have opposite signs in the upper layer.

V. TWO-DIMENSIONAL RESULTS FOR $U \neq 0$

Given the symmetries inherent to the mathematical problem we have solved, we confine the presentation of our results to those cases for which $U > 0$. The dispersion relation is now a complex expression, and it is given in Appendix A.

Figure 4 depicts the neutral curves corresponding to the first and second modes for the velocity differentials, $U = 0$, 0.5, 1, 1.5, and 2. The presence of the background counter-flow alters the morphology of the neutral curves from that which occurs when there is no flow. For any nonzero flow rate, no matter how small, there always exists a wavenumber at which modes 1 and 2 merge into a complex pair of travelling modes as k increases. This transition arises at the turning point in the neutral curves (i.e., where the tangent to the stationary-mode neutral curve is vertical) and it occurs at decreasing wavenumbers as the velocity differential, U, increases. The value of the Darcy-Rayleigh number at the turning point is denoted by Ra_{TP}.

The corresponding neutral curves for the larger velocity differentials $U = 2.859$, 4, and 6, are presented in Fig. 5. Although the general shape of these curves is the same as

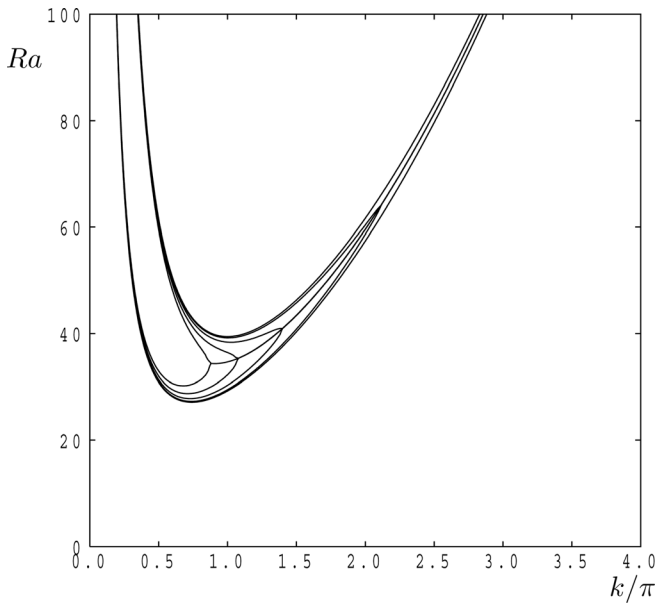


FIG. 4. The neutral curves corresponding to the first and second modes when $U = 0$ (outermost), 0.5, 1, 1.5, and 2 (innermost).

Downloaded 01 Aug 2011 to 138.38.54.38. Redistribution subject to AIP license or copyright; see http://pof.aip.org/about/rights_and_permissions

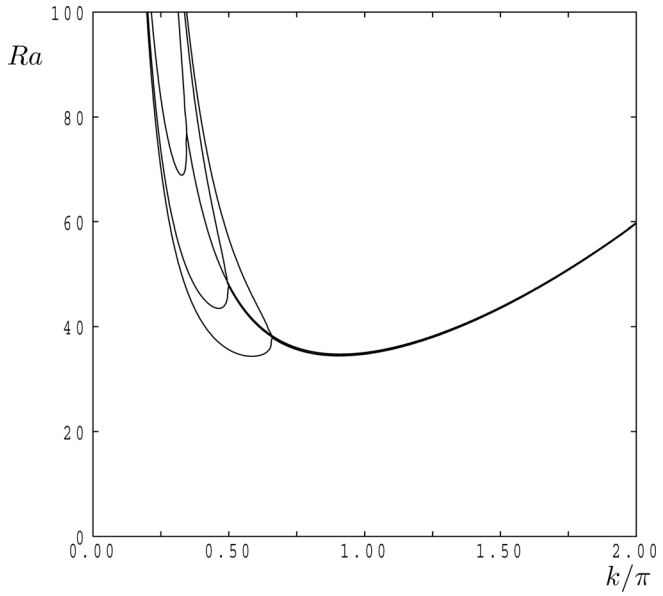


FIG. 5. The neutral curves corresponding to the first and second modes when $U = 2.859$, 4, and 6.

those shown in Fig. 4, the important difference is that the lowest value of Ra now corresponds to a pair of travelling waves. Indeed, the value $U = 2.859$ delineates the stationary convection regime ($U < 2.859$) from the travelling waves regime ($U > 2.859$). The critical Rayleigh number at this transitional value of U is $Ra_c = 34.322$ and the corresponding wavenumbers are $k = 0.585\pi$ (stationary) and $k = 0.906\pi$ (travelling).

It is quite clear from both Figs. 4 and 5 that the value of Ra for any chosen wavenumber for travelling modes varies very little as U varies, although the minimum value of the stationary part of the curves and the location of the turning point vary greatly. This is summarised graphically in Fig. 6, where we show the variation with U of the critical values (i.e., local minima) of the Rayleigh number for both stationary and travelling modes. Thus Ra_c increases slowly and in a parabolic-like manner as U increases, but then the critical mode switches suddenly to travelling modes and Ra_c is roughly constant. The reason for the roughly constant value of Ra_c for travelling modes is that the convection is now taking place almost exclusively in one sublayer and, therefore, the presence of the counterflow in the other sublayer affects the stability criterion only very slightly.

Figure 6 also shows the behaviour of the turning point in the stationary part of the neutral curve as U varies. This curve has its minimum when $U = 1.908$ and, therefore, the travelling mode part of the neutral curve has a minimum (in the sense that the derivative of Ra with respect to k is zero) only when $U > 1.908$. This may be understood more clearly with reference to the $U = 2$ curve in Fig. 4, where we see that the minimum in the travelling wave part of the curve is very close to the turning point in the stationary mode part of the curve. Thus the travelling mode branch shown in Fig. 6 emerges from the minimum in the travelling wave curve when $U = 1.908$.

When the value of U decreases towards zero, Fig. 6 shows clearly that the location of the turning point recedes towards infinity in both k and Ra, which we see in Fig. 4. A detailed analysis of this aspect is contained in Appendix B, but it is worth noting here that (i) the value of k at which the turning point may be found is given by $k^2 \sim 2\pi^2\sqrt{2}/U$ and (ii) the corresponding value of Ra is, to order k^{-1}, exactly midway between the critical values for modes 1 and 2, which are given in Eq. (19).

The wavenumbers corresponding to the Rayleigh numbers displayed in Fig. 6 are shown in Fig. 7. Here, we see the moderately slow reduction in the critical wavenumber for stationary modes as U increases, which was also seen in Fig. 4. Once the bullet symbol is encountered, then there is a sudden transition in the identity of the preferred mode to the travelling mode, and we see again that critical wavenumber hardly varies as U increases further. The travelling mode branch emerges from the turning point curve at $U = 1.908$, as discussed earlier.

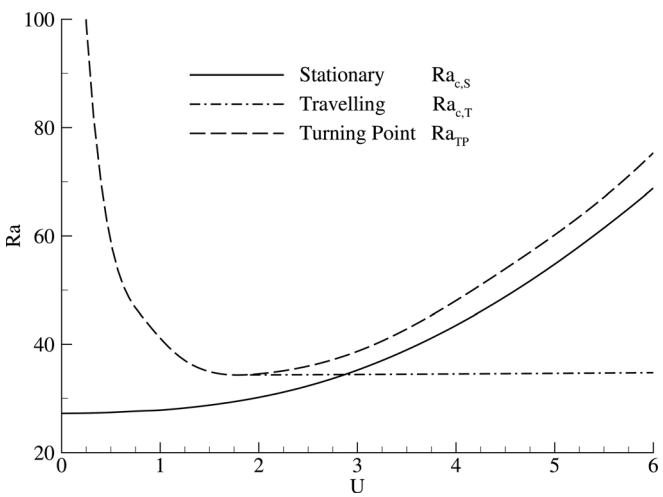


FIG. 6. Variation with U of the values of Ra corresponding to the turning point and to the minima in the neutral curve for both stationary and travelling modes.

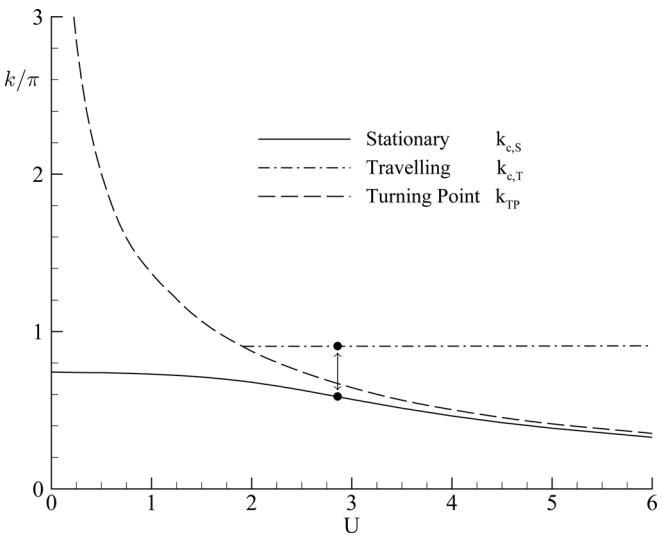


FIG. 7. Variation with U of the values of k/π corresponding to the turning point and to the minima in the neutral curve for both stationary and travelling modes. Also shown is the transition point between stationary and travelling waves forming the favoured mode (•).

Downloaded 01 Aug 2011 to 138.38.54.38. Redistribution subject to AIP license or copyright; see http://pof.aip.org/about/rights_and_permissions

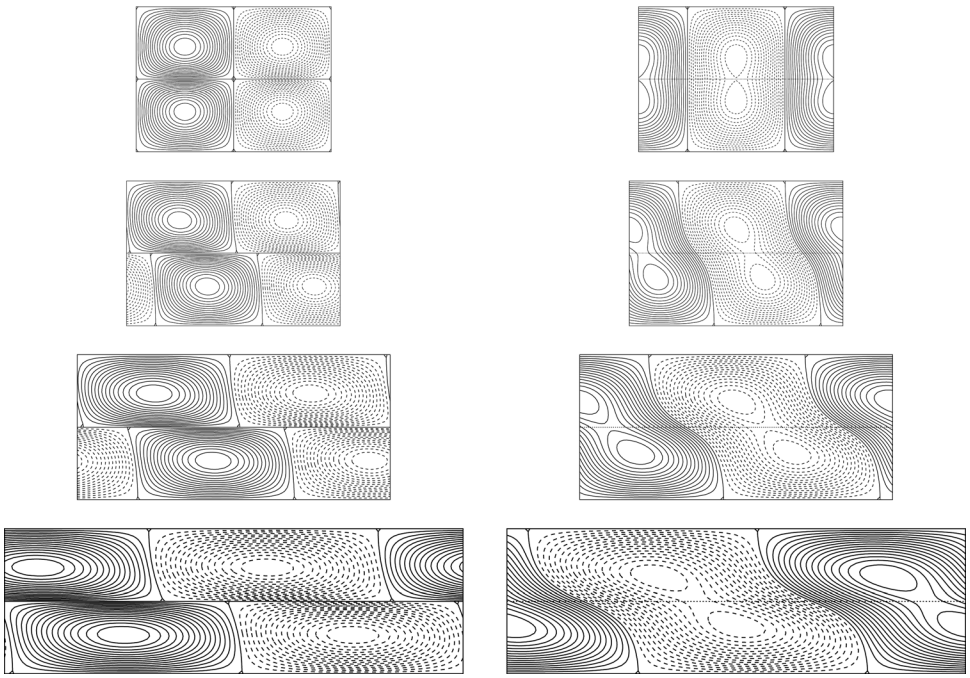


FIG. 8. Streamlines (left column) and isotherms (right column) for stationary mode convection for $U = 0$ (uppermost), 2, 4,and 6 (lowest).

Figure 8 shows the streamlines and isotherms corresponding to stationary modes for different values of U. When $U = 0$, the pattern corresponds to the critical mode, but for the other values of U, the pattern corresponds to the turning point. The width of each frame shows the precise aspect ratio of the pattern, given the value of the wavenumber. As U increases, an increasing distortion in the isotherms is induced, which indicates quite clearly that the background flow is from left to right in the lower layer and in the opposite direction in the upper layer. The streamlines display their own peculiar form of distortion by having the cells in one layer being displaced from their counterparts in the lower layer.

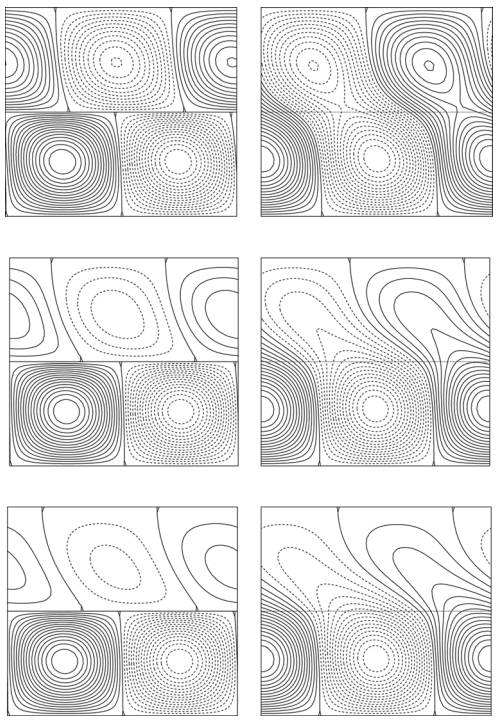


FIG. 9. Streamlines (left column) and isotherms (right column) for travelling mode convection for $U = 2$ (uppermost), 4, and 6 (lowest).

Figure 9 shows the streamlines and isotherms for travelling modes and these correspond to values of the Rayleigh number at the minimum of the travelling mode part of the neutral curves. When $U = 2$, there is very little difference between the strength of the pattern in the upper layer from that in the lower, but it is nevertheless discernable here. When U increases from this value, the convection pattern becomes concentrated increasingly within the lower layer, with only a weak contribution in the upper layer. Thus the patterns shown are a snapshot in time, and they represent modes which are moving to the right. Therefore, the pattern at a later time differs from what is shown by the distance it has travelled along the layer. The corresponding left-moving patterns are obtained by rotating these frames through 180°, and they have exactly the same critical Rayleigh number.

We also note that suitable combinations (i.e., the sum of equal-amplitude forms) of the two travelling waves will yield standing waves, which will oscillate in time with a periodic reversal of the direction of circulation of the convective cells. Whether this will arise in practice or whether travelling waves will be favoured can only be determined using a nonlinear analysis, which is outside the scope of the present work.

VI. THREE-DIMENSIONAL CASES

Finally, we generalise the two-dimensional cases considered already to ones where the horizontal direction of the flows in the sublayers take arbitrary directions. Now we shall allow the basic velocity fields in the sublayers to have the forms, $(u_j^{(b)}, v_j^{(b)})$ for $j = 1, 2$. The linear stability analysis presented earlier has to be reworked and the most convenient

Downloaded 01 Aug 2011 to 138.38.54.38. Redistribution subject to AIP license or copyright; see http://pof.aip.org/about/rights_and_permissions

form for this is in terms of the vertical velocity and temperature. The linearised stability equations, which are the three-dimensional equivalent of Eq. (11) are

$$\frac{\partial^2 W_j}{\partial x^2}+\frac{\partial^2 W_j}{\partial y^2}+\frac{\partial^2 W_j}{\partial z^2}=\mathrm{Ra}\left(\frac{\partial^2 \Theta_j}{\partial x^2}+\frac{\partial^2 \Theta_j}{\partial y^2}\right),$$
$$\frac{\partial \Theta_j}{\partial t}+u_j^{(b)}\frac{\partial \Theta_j}{\partial x}+v_j^{(b)}\frac{\partial \Theta_j}{\partial y}-W_j=\frac{\partial^2 \Theta_j}{\partial x^2}+\frac{\partial^2 \Theta_j}{\partial y^2}+\frac{\partial^2 \Theta_j}{\partial z^2}, \tag{22}$$

where W is the vertical velocity disturbance. Roll solutions corresponding to axes at an angle, γ, to the y-axis may now be introduced as follows:

$$W_j = -k f_j(z)\, e^{\lambda t+ik(x\cos\gamma-y\sin\gamma)},$$
$$\Theta_j = g_j(z)\, e^{\lambda t+ik(x\cos\gamma-y\sin\gamma)}, \tag{23}$$

where $\gamma = 0$ corresponds to the two-dimensional rolls considered above. Equations (22) now become,

$$f_j'' - k^2 f_j = Ra\, k\, g_j,$$
$$g_j'' - k^2 g_j - ik(u_j^{(b)}\cos\gamma - v_j^{(b)}\sin\gamma)g_j - k f_j = \lambda g_j, \tag{24}$$

and are subject to the boundary and interface conditions given in Eq. (14). Equation (24) reduces to the form given by Eq. (13) when $v_1^{(b)} = v_2^{(b)} = 0$. Thus, given the form of the coefficient of ikg_j in Eq. (24), and given that the critical value of Ra shown in Fig. 6 is an increasing function of U, it is clear that the minimising value of the roll orientation, γ, is that one for which the value of $(u_j^{(b)}\cos\gamma - v_j^{(b)}\sin\gamma)$ is the same in the two layers. This would then correspond to a situation where the two background velocity components, which are perpendicular to the roll orientation are equal to one another. Therefore we need,

$$u_1^{(b)}\cos\gamma - v_1^{(b)}\sin\gamma = u_2^{(b)}\cos\gamma - v_2^{(b)}\sin\gamma, \tag{25}$$

to be true, and this may be rearranged to yield,

$$\tan\gamma = \frac{u_1^{(b)} - u_2^{(b)\leftarrow}}{v_1^{(b)} - v_2^{(b)\leftarrow}}. \tag{26}$$

One example case is when the background flow is in the x-direction with strength, U, in layer 1 and in the y-direction also with strength, U, in layer 2. The above formula yields $\tan\gamma = -1$, and hence $\gamma = -45°$.

A second example is given by the two-dimensional cases considered earlier. If $u_1^{(b)}$ and $u_2^{(b)}$ take arbitrary values but $v_1^{(b)} = v_2^{(b)} = 0$, then $\gamma = 90°$, and the preferred rolls lie in the direction of the x-axis, rather than in the direction of the y-axis, which corresponds to the two-dimensional flow considered above.

In both these cases, when the optimum roll orientation forms the disturbance, the critical Darcy-Rayleigh number and the corresponding wavenumber correspond to when $U = 0$ for two-dimensional convection. Thus, for the transition to moving patterns to be observed in practice, it is essential that the flow is forced to be two-dimensional by restricting the width of the layer in the y-direction, or by considering the corresponding Hele-Shaw system.

VII. CONCLUSION

A linear stability analysis has been performed to determine the critical Darcy-Rayleigh number for the onset of convection in a horizontally partitioned porous layer heated from below with opposing horizontal pressure gradients. It has been shown that the stationary convection arises at onset when the velocity differential satisfies $U < 2.859$, but unsteady convection ensues otherwise. In dimensional terms, this means that stationary convection ensures when the seepage velocity is less than $2.859\kappa/H(\rho C)_f$. Streamline and isotherm patterns have also been given, and the detailed behaviour of the local minima and the turning point in the neutral curve have been presented.

When there is no background flow, then the critical value of the Darcy-Rayleigh number is $Ra_c = 2.74556\pi^2$, which is less than $4\pi^2$, the value for standard Darcy-Bénard layer. This appears to suggest that the presence of a partition reduces the critical value of Ra. However, if we had nondimensionalised using the full height of the layer and the temperature drop, then the corresponding critical value would be multiplied by 4 and would be $10.98224\pi^2$; all quoted wavenumbers would then be double the values quoted here. Thus, the presence of the partition increases the critical Darcy-Rayleigh number almost three-fold.

The present configuration bears some resemblance to the inclined form of the classical Darcy-Bénard problem, which has been studied by many (see, for example, Weber[13] and Caltagirone and Bories[14]) and, most recently, by Rees and Bassom.[12] The basic state in those papers consists of flow up the lower heated surface and down the upper cooled surface. Once the layer has been tilted away from the horizontal, stationary modes also coalesce into pairs of travelling waves, although these latter never form the most unstable state.

We make the following conclusions for cases, where the flow is constrained to be two-dimensional:

(1) The presence of the horizontal flow alters the morphology of the neutral curves from that which occurs when there is no flow.
(2) The value of the critical Darcy-Rayleigh number for stationary mode convection increases as the velocity differential, U, increases.
(3) The travelling mode branch of solutions bifurcates from a turning point formed by the merging of two stationary mode branches.
(4) The turning point recedes to infinity as $|U| \to 0$ and is asymptotically proportional to k^{-2} in that limit.
(5) Travelling modes are characterised by having convection concentrated primarily in only one of the sublayers.
(6) Travelling modes form the preferred mode of convection when $U > 2.895$.

When the fluid occupies a layer of infinite extent in both horizontal directions, and the background fluid velocities are

Downloaded 01 Aug 2011 to 138.38.54.38. Redistribution subject to AIP license or copyright; see http://pof.aip.org/about/rights_and_permissions

no longer parallel to one another, then the critical Darcy-Rayleigh corresponds to that roll orientation for which the perpendicular components of the background flows are identical and of the same sign. In such instances, the $U = 0$ result applies.

Finally, we need to make two comments on the realizability of the solutions we have found. First, we note that the configuration we have studied is structurally unstable in the sense that almost all slight perturbations to the system result in qualitative changes to the neutral curves. Examples of this include (i) a non-centrally located partition and (ii) slight changes in the permeability or diffusivity of one of the layers. In all of these cases, mode 1 would not retain its symmetry about the centre of the layer and the formerly stationary patterns would move. Likewise, our computed travelling wave solutions would now have unequal velocities in opposite directions and slightly different critical Darcy-Rayleigh numbers. Moreover, the morphology of the turning points would be altered.

Second, the configuration we have studied is of infinite horizontal extent, whereas any possible practical experimental work would involve finite layers. This would mean that the entrance effects would need to be taken into account in the analysis. Typically, disturbance quantities might be set to zero at inflow and, therefore, each of the sublayers would have a development region near the inflow boundary within which any upstream propagation of disturbances would die out. The papers by Dufour and Néel[15,16] consider this very situation for a single Darcy-Bénard layer. They show that the upstream propagation of disturbances is sufficiently strong that the entry region corresponds typically to only a few wavelengths of the convecting pattern. The length of the entry region increases with the strength of the background flow, but decreases as the Darcy-Rayleigh number increases. Therefore, we can conclude that our analysis could be modelled in the laboratory even if the length of the layer is not too large.

ACKNOWLEDGMENTS

G. G. wishes to thank the Erciyes University Foundation for supporting this work with a research fellowship, and the University of Bath for their hospitality. The authors would like to thank the reviewers for their excellent comments.

APPENDIX A: COMPLEX DISPERSION RELATION

If we set the exponential growth rate, λ, to be equal to ic, then the following is the dispersion relation for stationary convection when the velocity differential, U, is nonzero.

$$\frac{A_2\lambda_2\coth\lambda_2 - A_1\lambda_1\coth\lambda_1}{A_2 - A_1} + \frac{A_4\lambda_4\coth\lambda_4 - A_3\lambda_3\coth\lambda_3}{A_4 - A_3} = 0, \tag{A1}$$

where

$$A_1 = \frac{\lambda_1^2 - k^2 + i(c - ku_1^{(b)})}{k},$$

$$A_2 = \frac{\lambda_2^2 - k^2 + i(c - ku_1^{(b)})}{k},$$

$$A_3 = \frac{\lambda_3^2 - k^2 + i(c - ku_2^{(b)})}{k},$$

$$A_4 = \frac{\lambda_4^2 - k^2 + i(c - ku_2^{(b)})}{k},$$

and where

$$\lambda_1^2 = k^2 + \frac{(u_1^{(b)}k - c)i + \sqrt{4Rk^2 - (c - ku_1^{(b)})^2}}{2},$$

$$\lambda_2^2 = k^2 + \frac{(u_1^{(b)}k - c)i - \sqrt{4Rk^2 - (c - ku_1^{(b)})^2}}{2},$$

$$\lambda_3^2 = k^2 + \frac{(u_2^{(b)}k - c)i + \sqrt{4Rk^2 - (c - ku_2^{(b)})^2}}{2},$$

$$\lambda_4^2 = k^2 + \frac{(u_2^{(b)}k - c)i - \sqrt{4Rk^2 - (c - ku_2^{(b)})^2}}{2}.$$

When $u_1^{(b)} = -u_2^{(b)}$, which is the case we have considered, and when we are concerned solely with stationary modes, then we set $c = 0$. In such cases, $A_2 - A_1 = A_4 - A_1$, and the complex dispersion relation reduces to,

$$A_2\lambda_2\coth\lambda_2 - A_1\lambda_1\coth\lambda_1 + A_4\lambda_4\coth\lambda_4 - A_3\lambda_3\coth\lambda_3 = 0. \tag{A2}$$

This expression reduces still further to that given by Eq. (16) when $u_1^{(b)} = u_2^{(b)} = 0$.

APPENDIX B: TURNING POINT ANALYSIS FOR $|U| \ll 1$

The aim of this Appendix is to summarise briefly the analysis of the location of the turning point in the stationary part of the neutral curve as $U \to 0$. A detailed inspection of the numerically obtained values suggests that the appropriate balance of magnitudes is $U \propto k^{-2}$. The turning point must be located between the neutral stability curves for modes 1 and 2 for the stationary case, $U = 0$. Therefore, the analysis begins by setting,

$$Ra = k^2 + 2\pi^2 + \alpha k^{-1} + \cdots, \qquad U = \omega k^{-2}. \tag{B1}$$

The auxiliary quantites given in Appendix A become,

$$A_1 = k + \frac{\pi^2}{k} + \left(\frac{\alpha}{2} - \frac{\omega i}{4}\right)\frac{1}{k^2} + \cdots,$$

$$A_2 = -k - \frac{\pi^2}{k} + \left(\frac{\alpha}{2} - \frac{\omega i}{4}\right)\frac{1}{k^2} + \cdots,$$

$$A_3 = k + \frac{\pi^2}{k} + \left(\frac{\alpha}{2} + \frac{\omega i}{4}\right)\frac{1}{k^2} + \cdots,$$

$$A_4 = -k - \frac{\pi^2}{k} + \left(\frac{\alpha}{2} + \frac{\omega i}{4}\right)\frac{1}{k^2} + \cdots,$$

Downloaded 01 Aug 2011 to 138.38.54.38. Redistribution subject to AIP license or copyright; see http://pof.aip.org/about/rights_and_permissions

and

$$\lambda_1 = \sqrt{2}\left[k + \frac{\pi^2}{4k} + \left(\frac{\omega i}{16} + \frac{\alpha}{8}\right) + \cdots\right],$$
$$\lambda_2 = \pi i + \left(\frac{\omega}{8} + \frac{\alpha i}{4}\right)\frac{1}{\pi k} + \cdots,$$
$$\lambda_3 = \sqrt{2}\left[k + \frac{\pi^2}{4k} + \left(\frac{-\omega i}{16} + \frac{\alpha}{8}\right) + \cdots\right],$$
$$\lambda_4 = \pi i + \left(\frac{-\omega}{8} + \frac{\alpha i}{4}\right)\frac{1}{\pi k} + \cdots.$$

After substitution of these expressions into the dispersion relation Eq. (A2), we obtain the following formula at leading order:

$$\omega^2 = -4[2\sqrt{2}\pi^2\alpha + \alpha^2]. \tag{B2}$$

It is clear that ω^2 takes positive values only when

$$-2\sqrt{2}\pi^2 \le \alpha \le 0, \tag{B3}$$

which corresponds exactly to the region between the neutral curves for modes 1 and 2, which are given by the $O(k^{-1})$ terms in Eq. (19). Both extremes of this interval correspond to $\omega \to 0$, so that we recover one or the other of the first two modes for $U = 0$. The largest value of ω arises when $\alpha = -\sqrt{2}\pi^2$, for which the turning point corresponds to $\omega = 2\sqrt{2}\pi^2$. In terms of the original unscaled variables, the turning point arises at,

$$Ra_{\mathrm{TP}} \sim k^2 + 2\pi^2 - \sqrt{2}\pi^2 k^{-1}, \qquad k_{\mathrm{TP}} \sim 2\sqrt{2}\pi^2/U, \tag{B4}$$

when $U \ll 1$.

[1] C. W. Horton and F. T. Rogers, "Convection currents in a porous medium," J. Appl. Phys. **16**, 367 (1945).
[2] E. R. Lapwood, "Convection of a fluid in a porous medium," Proc. Cambridge Philos. Soc **44**, 508 (1948).
[3] M. Prats, "The effect of horizontal fluid motion on thermally induced convection currents in porous mediums," J. Geophys. Res. **71**, 4835 (1966).
[4] R. McKibbin and M. J. O'Sullivan, "Onset of convection in a layered porous medium heated from below," J. Fluid Mech. **96**, 375 (1980).
[5] R. McKibbin and M. J. O'Sullivan, "Heat transfer in a layered porous medium heated from below," J. Fluid Mech. **111**, 141 (1981).
[6] D. A. S. Rees and D. S. Riley, "The three-dimensional stability of finite-amplitude convection in a layered porous medium heated from below," J. Fluid Mech. **211**, 437 (1989).
[7] D. N. Riahi, "Nonlinear convection in a porous layer with finite conducting boundaries," J. Fluid Mech. **129**, 153 (1983).
[8] T. Masuoka, T. Katsuhara, Y. Nakazono, and S. Isozaki, "Onset of covection and flow patterns in a porous layer of two different media," Heat Transfer-Jpn. Res. **7**, 39 (1979).
[9] R. Rana, R. N. Horne, and P. Cheng, "Natural convection in a multi-layered geothermal reservoir," J. Heat Transfer **101**, 411 (1979).
[10] R. McKibbin, "Convection in an aquifer above a layer of heated impermeable rock," N. Z. J. Sci. **26**, 49 (1983).
[11] J. Y. Jang and W. L. Tsai, "Thermal instability of two horizontal porous layers with a conductive partition," Int. J. Heat Mass Transfer **31**, 993 (1988).
[12] D. A. S. Rees and A. P. Bassom, "Onset of Darcy-Bénard convection in an inclined porous layer heated from below," Acta Mech. **144**, 103 (2000).
[13] J. E. Weber, "Thermal convection in a tilted porous layer," Int. J. Heat Mass Transfer **18**, 474 (1975).
[14] J.-P. Caltagirone and S. A. Bories, "Solutions and stability criteria of natural convective flow in an inclined porous layer," J. Fluid Mech. **155**, 267 (1985).
[15] F. Dufour and M.-C. Néel, "Numerical study of instability in a horizontal porous channel with bottom heating and forced horizontal flow," Phys. Fluids **10**, 2198 (1998).
[16] F. Dufour and M.-C. Néel, "Time-periodic convective patterns in a horizontal porous layer with through-flow," Q. Appl. Math. **58**, 265 (2000).

Downloaded 01 Aug 2011 to 138.38.54.38. Redistribution subject to AIP license or copyright; see http://pof.aip.org/about/rights_and_permissions